



Reactive scattering of O^+ on oxidized Si(001)

C.L. Quinteros, T. Tzvetkov, X. Qin, D.C. Jacobs *

Department of Chemistry and Biochemistry, University of Notre Dame, Notre Dame, IN 46556, USA

Abstract

Thin silicon oxide films are grown on Si(001) through ion-beam oxidation (IBO), using hyperthermal O^+ ions. Within a steady-state oxidation regime, scattering of O^+ from these thin films yields both positive (Si^+ , SiO^+) and negative (O^- , O_2^-) ion products. The emergence of O^- and O_2^- is investigated through isotopic labeling and angle-, mass- and energy-resolved detection. The O^- signal comprises direct scattering and surface recoil components. Two distinct O_2^- formation mechanisms are operative, with different dependencies on incident O^+ energy: at low O^+ energies, O_2^- is created exclusively by abstraction of a surface oxygen atom by an incident oxygen; whereas for higher O^+ energies, a second channel involving a recoil abstracting a surface atom contributes. These studies represent the first investigation of the scattered reaction products formed during silicon IBO. © 2001 Published by Elsevier Science B.V.

1. Introduction

The oxidation of silicon surfaces by hyperthermal oxygen ions ($E < 1000$ eV) has been studied both experimentally and theoretically as an alternative pathway to thermal oxidation in semiconductor applications [1–8]. The main advantage of using hyperthermal oxygen ions over traditional thermal silicon oxidation is the ability to synthesize thicker oxide films without resorting to high-temperature annealing to overcome oxygen diffusion limits. Low-temperature IBO, where the kinetic energy of the incident ion activates oxygen diffusion, has important advantages in terms of device reliability: lower processing tem-

peratures minimize electromigration and dopant diffusion problems, reducing device failure.

Most of the studies on this technique have focused on characterizing thin silicon oxide films produced by IBO; i.e., measuring the dependence of film properties on important process parameters such as oxygen ion energy, oxidation temperature, and incident angle [1,9,10]. Todorov and Fosum [11] have reported that 40–200 eV oxygen ions incident on Si(001) produce an oxide film, saturating at 4 nm thickness.

Vancauwenberghe et al. [4] have extensively studied the oxidation and nitridation of silicon, germanium and silicon-germanium alloys by ion-beam synthesis. Their studies indicate that the interface properties of the silicon/silicon oxide films, and the stoichiometry of the oxide itself are comparable to those found on films produced through thermal silicon oxidation methods. They also observe a saturation in film thickness for high ion

* Corresponding author. Tel.: +1-219-631-8023; fax: +1-219-631-6652.

E-mail address: jacobs.2@nd.edu (D.C. Jacobs).

doses and a sharp oxide–substrate interface. The oxygen dose needed to reach this saturation regime and the saturation thickness achieved are dependent on the incident oxygen energy. Shibata et al. [12] used a combined 50 eV O^+ ion-beam/molecular-beam epitaxial method (CIBMBE) and concluded, based on their XPS studies, that the properties of the oxide film were comparable to a thermally grown oxide.

A series of different models were developed to explain the experimental results for IBO of silicon [1,13]. To accurately account for the sharp interface, the saturation thickness, and its dependence on the incident ion energy, it was necessary to consider not only the mechanisms of deposition and sputtering, but also the rates of oxidation, replacement, and relocation events, as well as thermal and ion-beam enhanced oxygen diffusion.

This work aims to establish the different chemical reactions that are operative in the IBO steady-state oxidation regime. Mechanistic information is derived from an analysis of the angular-, mass-, and energy-resolved distributions of scattered products as a function of incident energy.

2. Experimental

The experimental apparatus comprises three differentially pumped chambers. The O^+ beam is created in the source chamber, by the extraction of positive ions from a Colutron plasma source. The feed gas is CO_2 , because it produces predominantly ground-state $O^+(^4S)$ [14]. The extracted ions are focused and accelerated to 1300 eV to minimize space charge effects during transport to the scattering chamber. A Wien filter and flight tube are used to mass-filter the O^+ beam. A deflection stage within the buffer chamber eliminates any surviving neutralized hyperthermal particles. In the main chamber, the O^+ beam is decelerated to its final energy, 10–150 eV, before striking the silicon surface. Ion-beam current densities are 40–120 nA/cm² at the target. The main chamber pressure during the experiments remains at 6×10^{-10} Torr. Scattered ionic products are mass- and energy-analyzed with a rotatable, differentially pumped detector including a cylindrical electro-

static analyzer, a quadrupole mass spectrometer, and a pair of microchannel plates for single-particle detection.

Surface samples (Chochralsky grown, p-doped Si(001); $R = 0.01\text{--}0.02 \Omega \text{ cm}$) are cleaned by chemical oxidation, followed by hydrogen-termination in buffered HF [15]. The sample is introduced into the main chamber through a load-lock. Low-energy electron diffraction (LEED) reveals a clean, well-ordered (2×1) structure after annealing at 900°C. Contamination removal is confirmed by in situ XPS.

The clean surface is exposed to the O^+ beam at 45° incidence. A silicon oxide film grows until it reaches the steady-state regime, where the rate of oxygen incorporation is balanced by oxygen removal from the outermost layers of the film. Scattering of O^+ from these thin films yields both positive (Si^+ , SiO^+) and negative (O^- , O_2^-) ion products. Scattered O^+ is not observed, indicating efficient neutralization along the inbound trajectory [5,6]. It was confirmed by XPS that, as the intensity of the scattered O^- and O_2^- signal increases, the oxide also develops. An isotopic labeling approach was used to distinguish between oxygen entities originating from the surface and those from the incident ion beam. Thin silicon oxide films were grown with an isotopically pure $^{16}O^+$ beam directed at the Si(001) surface. Once the saturation regime was reached, the energy- and angular-distributions of the scattered products were recorded using a mass-filtered $^{18}O^+$ beam.

3. Results and discussion

The negative ion (O^- and O_2^-) signals include oxygen contributions from both the surface and the incident ion beam. In the case of O^- , the mass-resolved components are easily identified as either scattered projectiles ($18 \text{ u} = ^{18}O^-$) or recoiled/sputtered surface oxygen ($16 \text{ u} = ^{16}O^-$). The origin of each oxygen atom in the O_2^- products is also unambiguously identified. For $^{18}O^+$ incident energies up to 60 eV and scattering angles between 45° and 135°, 98 ± 1% of the scattered O_2^- appears at mass-34. Therefore, O_2^- is formed with a combination of one oxygen atom from the incident ion

beam (^{18}O) and one oxygen atom from the silicon oxide layer (^{16}O). The lack of signal corresponding to $^{32}\text{O}_2^-$ and $^{36}\text{O}_2^-$ precludes physical sputtering and projectile recombination, respectively, as possible mechanisms for O_2^- formation at these low energies [16].

Extending the range of incident energies up to 150 eV opens a new O_2^- formation channel: $^{32}\text{O}_2^-$ is generated with two oxygen atoms originating from the surface. Fig. 1 shows the yield of each O_2^- product channel as a function of the incident energy. The mass-34 component shows a threshold of 16 eV, indicative of a reaction barrier above which the reaction probability increases. However, O_2^- can suffer electron autodetachment when the molecular anion's vibrational energy exceeds $\nu = 3$ (~ 0.5 eV) [17]. As the incident energy increases, the vibrational energy of the product is more likely to exceed the autodetachment limit, leading to neutralization and reduction of the nascent O_2^- signal above 60 eV. The formation of $^{32}\text{O}_2^-$ exhibits an energy threshold of 33 ± 3 eV. Unlike its counterpart, $^{32}\text{O}_2^-$ monotonically increases, suggestive that $^{32}\text{O}_2^-$ emerges vibrationally colder than does $^{34}\text{O}_2^-$.

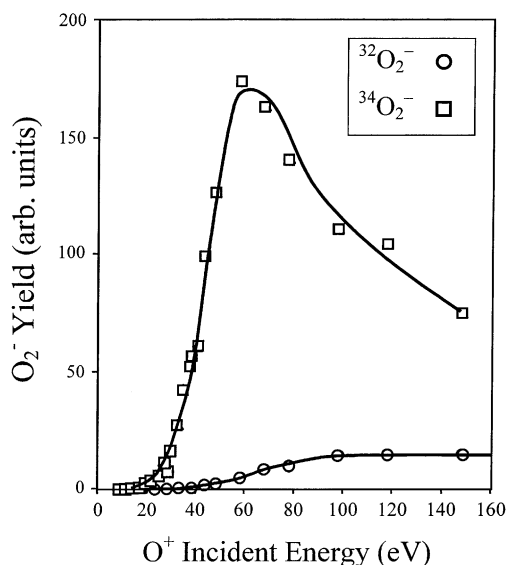


Fig. 1. Yields of $^{32}\text{O}_2^-$ and $^{34}\text{O}_2^-$ for O^+ incident on $\text{SiO}_x/\text{Si}(001)$. The thresholds for $^{34}\text{O}_2^-$ and $^{32}\text{O}_2^-$ emergence are 16 ± 1 eV and 33 ± 3 eV, respectively.

Fig. 2 shows the mean translational energy of the scattered O_2^- products, averaged over all measured scattering angles (45° – 135°). A correlation with incident energy is apparent for both channels. The average energy for $^{32}\text{O}_2^-$ products is ~ 2 – 3 eV lower than for $^{34}\text{O}_2^-$ at all incident energies.

Both $^{32}\text{O}_2^-$ and $^{34}\text{O}_2^-$ channels show strong forward scattering in the angular distributions demonstrating that neither product is formed as a consequence of indirect cascade sputtering. At these low energies, the penetration depth of the incident particle is quite shallow (only a few monolayers). Thus, direct scattering, recoiling and short cascades (a few collisions) are most likely [18,19]. Previous modeling of IBO indicated that the origin of the recoils usually involved the first two or three surface layers [1]. Moreover, cascade sputtering would produce low-energy products, which are less likely to survive as negative ions and be collected.

Possible reaction mechanisms leading to scattered O_2^- are depicted in Fig. 3. Figs. 3(a) and (b) illustrate two proposed mechanisms for $^{34}\text{O}_2^-$ formation. Fig. 3(a) represents a direct, single collision abstraction mechanism, while Fig. 3(b) depicts scattering-mediated abstraction [20]. In the

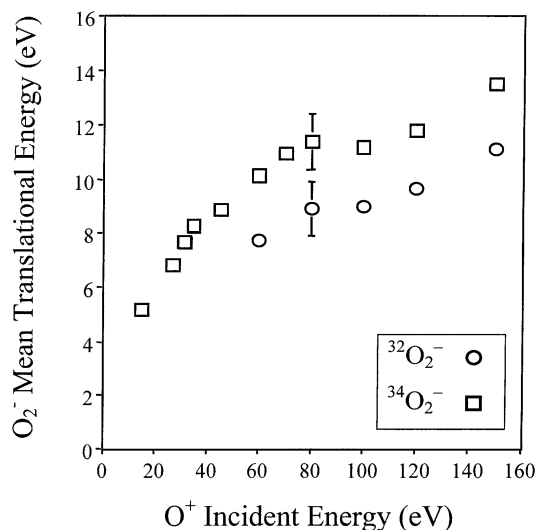


Fig. 2. Mean exit energy of $^{32}\text{O}_2^-$ and $^{34}\text{O}_2^-$ products vs. O^+ incident energy.

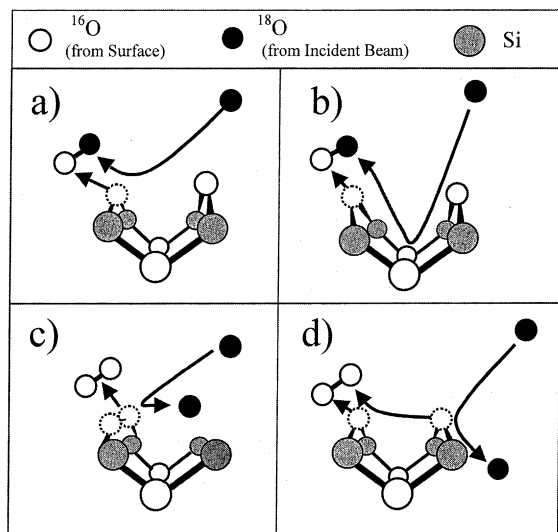


Fig. 3. Proposed mechanisms for O_2^- emergence. (a) Direct oxygen abstraction. (b) Scattering-mediated oxygen abstraction. (c) Sputtering of a peroxyl bridge surface species. (d) Recoil-abstraction: an ^{16}O recoil from the surface abstracts a neighboring O-atom.

second case, the incident atom collides with the substrate before abstracting a surface O-atom along the outbound trajectory. The entire trajectory must not involve too many collisions with the surface, because the angular distribution of the scattered $^{34}\text{O}_2^-$ product appears highly correlated with the incident angle [16].

Evidence that O_2^- is formed as a molecular anion, and not as a neutral molecule that picks up an electron on the outgoing trajectory, is deduced from scattering experiments with incident $^{36}\text{O}_2^+$ [21]. For 60 eV $^{36}\text{O}_2^+$ incident on Si^{16}O_x , the normalized yield of scattered $^{36}\text{O}_2^-$ (resulting from a transfer of two electrons from the surface) is $\sim 1/4$ of the $^{34}\text{O}_2^-$ normalized yield when 60 eV $^{18}\text{O}^+$ is used as the incident projectile. If the latter reaction comprised a neutral abstraction step followed by electron attachment to the nascent O_2 product, the yield of $^{34}\text{O}_2^-$ from incident $^{18}\text{O}^+$ should be much lower than the direct scattering yield of $^{36}\text{O}_2^-$ from incident $^{36}\text{O}_2^+$. However, the opposite result is observed. Therefore, it is reasonable to assume that the abstraction product ($^{34}\text{O}_2^-$) is formed directly as an *anion* at the surface.

Sputtering of physisorbed O_2 is discounted as a possible source for $^{32}\text{O}_2^-$, because the sputtering of a physisorbed molecular species should have a much lower threshold than 33 eV (where $^{32}\text{O}_2^-$ first appears). Furthermore, the presence of molecular oxygen on the surface, for a timescale long enough and at large enough concentrations so as to produce a high $^{32}\text{O}_2^-$ signal, is contrary to IBO modeling studies [1]. Fig. 3(c) depicts a mechanism for forming $^{32}\text{O}_2^-$ through sputtering of a peroxyl group. The existence of peroxyl bridges in silica is supported by both experimental and theoretical studies [22–26]. The IBO process is rich in oxygen and energy, and defects are paramount to the film's growth. In fact, several different oxygen moieties may be present in the IBO films, e.g., Si–O–Si bridges [27], interstitial oxygen [27], peroxy radicals, [24,28,29] and Si–O–O–Si structures [30,31].

Fig. 3(d) shows a second plausible mechanism for the formation of $^{32}\text{O}_2^-$, namely recoil-abstraction. Here the incident projectile dislodges an energetic ^{16}O recoil that, in turn, collides and reacts with another O-atom from the surface. The latter half of this mechanism resembles the surface-mediated abstraction event depicted in Fig. 3(b). A recoil-abstraction process would not necessarily follow the simple two-collision pathway depicted in the cartoon, but might include multiple bounces on the surface.

Further insight into the mechanism of $^{32}\text{O}_2^-$ emergence is achieved by analyzing the yields of the O^- species leaving the surface. For the mechanisms depicted in Figs. 3(b) and (d), the precursor to abstraction is O^- on its outbound trajectory. Only a fraction of the outgoing O^- (scattered $^{18}\text{O}^-$ and $^{16}\text{O}^-$ recoils in Figs. 3(b) and (d), respectively) will successfully abstract O from the surface to form O_2^- . Thus, if scattering-mediated abstraction and recoil-abstraction are the operative mechanisms for O_2^- formation, the $^{32}\text{O}_2^-$ and $^{34}\text{O}_2^-$ yields should be correlated with those for the corresponding emerging precursors, $^{16}\text{O}^-$ and $^{18}\text{O}^-$, respectively. Fig. 4 shows the yields of scattered $^{16}\text{O}^-$, $^{18}\text{O}^-$, $^{32}\text{O}_2^-$ and $^{34}\text{O}_2^-$ products versus incident energy. Both $^{18}\text{O}^-$ and $^{34}\text{O}_2^-$ rise steeply with incident energy and plateau near ~ 50 eV. The reduction in slope for the $^{18}\text{O}^-$ yield at

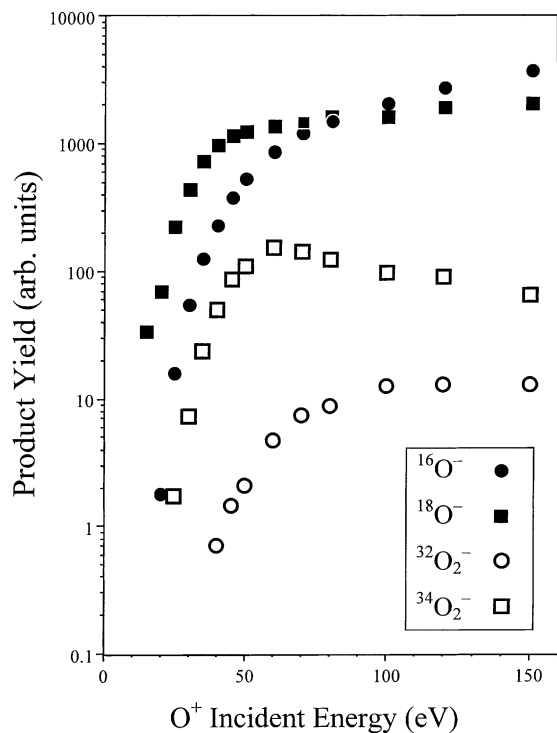


Fig. 4. $^{16}\text{O}^-$, $^{18}\text{O}^-$, $^{32}\text{O}_2^-$ and $^{34}\text{O}_2^-$ yields for O^+ incident on $\text{SiO}_x/\text{Si}(001)$ as a function of the $^{18}\text{O}^+$ incident energy.

O^+ energies higher than ~ 60 eV can be attributed to a higher probability for projectile implantation with increased projectile energy. As mentioned previously, the decay in the yield of $^{34}\text{O}_2^-$ for $E_i(\text{O}^+) > 60$ eV can be interpreted as an increase in the electron autodetachment probability for more vibrationally excited products. The similar shape in the $^{18}\text{O}^-$ and $^{34}\text{O}_2^-$ yield curves is consistent with scattered $^{18}\text{O}^-$ being the precursor to $^{34}\text{O}_2^-$ formation, in support of the scattering-mediated abstraction mechanism. Likewise, $^{16}\text{O}^-$ and $^{32}\text{O}_2^-$ exhibit similar curvatures up to collision energies of 100 eV. Thereafter, the $^{32}\text{O}_2^-$ yields plateau, while the $^{16}\text{O}^-$ yield keeps continuing to rise. An increase in the electron autodetachment probability for higher incident O^+ energies can again explain this difference between precursor and molecular product yields. The clear correlation between O_2^- and O^- yields for both product channels suggests that scattered $^{18}\text{O}^-$ and $^{16}\text{O}^-$ are precursors to abstraction along the outgoing

trajectory, as illustrated in Figs. 3(b) and (d), respectively.

The question remains as to whether neutral O may also serve as a precursor to abstraction in the formation of O_2^- . The $^{18}\text{O}^-$ yield curve in Fig. 4 represents the direct scattering component. The absence of $^{18}\text{O}^-$ signal for $E_{\text{inc}}(^{18}\text{O}^+) < 12$ eV, and the steep increase for O^+ energies up to 60 eV, is consistent with an increased survival probability for O^- with increasing O^- final energy. The neutral oxygen scattered signal, on the other hand would lack the filtering effect of electron loss with decreasing O^- final energy. It is reasonable to assume that the scattered neutral ^{18}O yield (direct scattering component) would be highest for low O^+ incident energies, and decrease as projectile implantation becomes activated by incident energy. Thus, the yield curve for neutral ^{18}O -atoms should be fundamentally different than that observed for $^{18}\text{O}^-$ anions (Fig. 4) and uncorrelated with that for $^{34}\text{O}_2^-$ products. The parallel curves in Fig. 4 suggest that a scattered O^- anion rather than a neutral O-atom serves as the precursor to abstraction in O_2^- emergence. Furthermore, the strong correlation between the O^- and O_2^- angular distributions is consistent with O^- being the precursor to O_2^- formation in both the scattering-mediated and recoil-abstraction channels [21].

4. Summary

Hyperthermal O^+ reacts with an $\text{SiO}_x/\text{Si}(001)$ thin film to produce scattered O^- and O_2^- . Isotropic labeling permits the independent study of each contributing mechanism. Both scattered projectiles and surface recoils form the O^- signal. At low energies, O_2^- is produced exclusively by scattering-mediated abstraction, where a scattered O^- anion reacts with a surface O-atom. At higher energies, recoil-abstraction is observed, in which a recoiling O^- anion collides with a neighboring surface O-atom to form O_2^- . The two mechanisms are related in that scattering-mediated abstraction and recoil-abstraction both form O_2^- products along the outgoing path of the trajectory.

Acknowledgements

Support from the Air Force Office of Scientific Research is gratefully acknowledged.

References

- [1] O. Vancauwenberghe, N. Herbots, O.C. Hellman, J. Vac. Sci. Technol. A 10 (1992) 713.
- [2] N. Herbots, O.C. Hellman, P. Ye, X. Wang, O. Vancauwenberghe, in: J.W. Rabalais (Ed.), *Low Energy Ion–Surface Interactions*, Wiley, New York, 1994 (Chapter 8).
- [3] N. Herbots, O. Vancauwenberghe, O.C. Hellman, Y.C. Joo, Nucl. Instr. and Meth. B 59 (1991) 326.
- [4] O. Vancauwenberghe, O.C. Hellman, N. Herbots, W.J. Tan, J.L. Olson, W.J. Croft, Mater. Sci. Eng. B 12 (1992) 97.
- [5] J.H. Rechten, U. Imke, K.J. Snowdon, P.H.F. Reijnen, P.J.v.d. Hoek, A.W. Kleyn, A. Namiki, Nucl. Instr. and Meth. B 48 (1990) 339.
- [6] J.H. Rechten, U. Imke, K.J. Snowdon, P.H.F. Reijnen, P.J.v.d. Hoek, A.W. Kleyn, A. Namiki, Surf. Sci. 227 (1990) 35.
- [7] A.H. Al-Bayati, S.S. Todorov, K.J. Marton, J.W. Rabalais, J. Vac. Sci. Technol. B 13 (1995) 1639.
- [8] B.C. Kim, J.R. Hahn, H. Kang, Nucl. Instr. and Meth. B 106 (1995) 137.
- [9] N. Herbots, O.C. Hellman, P.A. Cullen, O. Vancauwenberghe, in: G.W. Rubloff (Ed.), *Deposition and Growth: Limits for Microelectronics*, Vol. 167, American Vacuum Society Series 4, AIP, 1988, p. 259.
- [10] W. Vandervost, in: M.A. Nastasi, N. Herbots, L.H. Harriot, R. Averbach (Eds.), *Beam–Solid Interactions: Fundamentals and Applications*, Mater. Sci. Res. Soc. Symp. Proc. 259, 1993.
- [11] S.S. Todorov, E.R. Fosum, Appl. Phys. Lett. 52 (1988) 48.
- [12] H. Shibata, S. Kimura, H. Takatoh, Jpn. J. Appl. Phys. 39 (2000) 1327.
- [13] S.S. Todorov, I.R. Chakarov, D.S. Karpuzov, Nucl. Instr. and Meth. B 65 (1992) 79.
- [14] B.M. Huges, T.O. Tiernan, J. Chem. Phys. 55 (1971) 3419.
- [15] P. Dumas, Y.J. Chabal, P. Jakob, P. Dumas, Surf. Sci. 270 (1992) 867.
- [16] C.L. Quinteros, T. Tzvetkov, D.C. Jacobs, J. Chem. Phys. 113 (2000) 5119.
- [17] R.J. Celotta, R.A. Bennett, J.L. Hall, M.W. Siegel, J. Levine, Phys. Rev. A 6 (1972) 631.
- [18] P. Varga, U. Diebold, in: J.W. Rabalais (Ed.), *Low Energy Ion–Surface Interactions*, Wiley, New York, 1994, Chapter 7.
- [19] H. Gnaser, *Low-Energy Ion Irradiation of Solid Surfaces*, Springer, Berlin, 1999, p. 49.
- [20] S.I. Yi, W.H. Weinberg, Surf. Sci. 415 (1998) 274.
- [21] T. Tzvetkov, C.L. Quinteros, X. Qin, D.C. Jacobs, In preparation.
- [22] G. Pacchioni, G. Ierano, Phys. Rev. B 56 (1997) 7304.
- [23] E.P. Oreilly, J. Robertson, Phys. Rev. B 27 (1983) 3780.
- [24] H. Nishikawa, R.Y. Ohki, Y. Hama, Phys. Rev. B 48 (1993) 15584.
- [25] H. Imai, K. Arai, H. Hosono, Y. Abe, T. Arai, H. Imagawa, Phys. Rev. B 44 (1991) 4812.
- [26] H. Nishikawa, R. Tohmon, Y. Ohki, K. Nagasawa, Y. Hama, J. App. Phys 65 (1989) 4672.
- [27] J. Dabroski, H.J. Mussig, *Silicon Surfaces and Formation of Interfaces*, World Scientific, Singapore, 2000.
- [28] B.L. Zang, K. Raghavachari, Phys. Rev. B 55 (1997) R15993.
- [29] L. Skuja, B. Güttler, Phys. Rev. Lett. 77 (1996) 2093.
- [30] J.R. Chelikowsky, D.J. Chadi, N. Binggeli, Phys. Rev. B 62 (2000) R2251.
- [31] L. Skuja, M. Hirano, H. Hosono, Phys. Rev. Lett. 84 (2000) 302.